6 Equivalent circuits and methods to determine the system parameters

For the clear specification of the electromagnetic processes in 3-phase AC machines and as a starting point for control design, equivalent circuits which are based on the representation of the physical quantities as complex space vectors *in a stator-fixed coordinate system* will be a very useful tool. The underlying mathematics is strongly related to the complex calculations known from the AC technology. To abstract the physical operation of the machines, inductances and resistances are represented as concentrated components, and symmetrical conditions are assumed with regard to the 3-phase windings.

For the satisfactory function of a controller designed using equivalent circuits the parameters of the equivalent circuits must be known with sufficient accuracy. From modern drives it will be expected that they fulfill the projected quality parameters without special tuning to be carried out by the customer, and keep the parameters durably. Because frequency converters, particularly in small and medium power ranges, are offered in principle as separate units without motors, parameter pre-setting or measuring the used motor by means of classical methods (no-load or short circuit test) are not practicable. Therefore the second part of this chapter deals with possibilities of the automated computation of the electrical motor parameters.

A first starting-point and also a base for start values of a more exact estimation will be provided by the name plate or by the rated data of the motor. For a more exact parameter setting off-line identification methods which provide estimated values of motor parameters during a test run in standstill are discussed.

6.1 Equivalent circuits with constant parameters

6.1.1 Equivalent circuits of the IM

6.1.1.1 T equivalent circuit

The general voltage and flux-linkage equations in the stator-fixed coordinate system (cf. chapter 3)

$$\mathbf{u}_s = R_s \mathbf{i}_s + \dot{\boldsymbol{\psi}}_s \tag{6.1}$$

$$\mathbf{u}_r^r = R_r^r \mathbf{i}_r^r + \dot{\boldsymbol{\psi}}_r^r - j\omega\, \boldsymbol{\psi}_r^r \tag{6.2}$$

$$\boldsymbol{\psi}_s = L_s \mathbf{i}_s + L_m \mathbf{i}_r \tag{6.3}$$

$$\boldsymbol{\psi}_r^r = L_r^r \mathbf{i}_r^r + L_m^r \mathbf{i}_s^r \tag{6.4}$$

describe a transformer with an additional secondary (rotor-sided) voltage source as represented in figure 6.1. In this case the superscript r means that the so labelled parameters and quantities are related to the rotor side, and therefore correspond to the values measured at rotor terminals physically. Quantities without such index are related to the stator side.

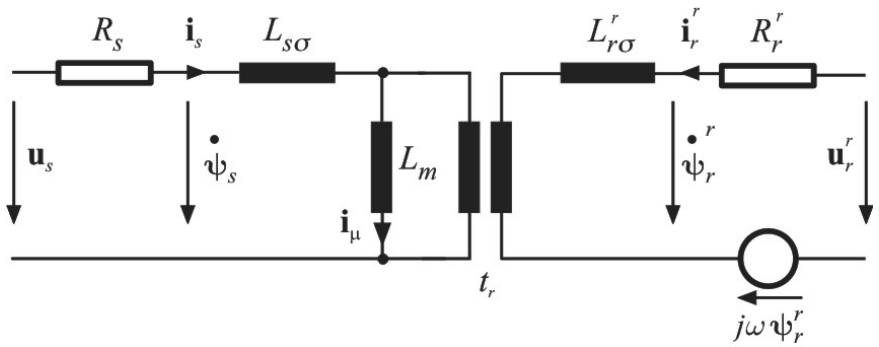

Fig. 6.1 Transformer-equivalent circuit of the induction machine

The actual transformer symbol in the equivalent circuit marks an ideal transformer with the transfer ratio t_r. This contains the turn ratio and winding factors, and can be expressed by the relationship between the no-load nominal voltages.

$$t_r = \frac{U_{rN}}{U_{sN}} \tag{6.5}$$

Because the induction machine is fed normally from either the stator side or the rotor side, it is usual and useful to relate all electrical quantities to either the stator side or the rotor side. Subsequently, on principle, the stator side reference shall be used. For the transformation of the rotor quantities to the stator side the following relations are obtained by using the transfer ratio t_r defined above:

$$\begin{aligned} \mathbf{u}_r &= \frac{\mathbf{u}_r^r}{t_r} \\ \mathbf{i}_r &= t_r\,\mathbf{i}_r^r \\ \psi_r &= \frac{\psi_r^r}{t_r} \end{aligned} \tag{6.6}$$

$$\begin{aligned} R_r &= \frac{R_r^r}{t_r^2} \\ L_r &= \frac{L_r^r}{t_r^2} \end{aligned} \tag{6.7}$$

For the current through the main inductance L_m (the magnetizing current $\mathbf{i}_\mu$) can be written:

$$\mathbf{i}_\mu = \mathbf{i}_s + \mathbf{i}_r \tag{6.8}$$

The reference to the stator side is primarily relevant for the treatment of the squirrel-cage IM ($\mathbf{u}_r = 0$) which shall be also the object of the further derivations. Because of the interchangeability of both approaches this does not represent any essential restriction of the generality.

If the flux-linkage in (6.1), (6.2) is replaced by (6.3), (6.4), the equations of the stator and rotor voltage can be changed into the form:

$$\mathbf{u}_s = R_s\mathbf{i}_s + L_{s\sigma}\frac{\mathrm{d}\mathbf{i}_s}{\mathrm{d}t} + L_m\frac{\mathrm{d}\mathbf{i}_\mu}{\mathrm{d}t} \tag{6.9}$$

$$0 = R_r\mathbf{i}_r + L_{r\sigma}\frac{\mathrm{d}\mathbf{i}_r}{\mathrm{d}t} + L_m\frac{\mathrm{d}\mathbf{i}_\mu}{\mathrm{d}t} - j\omega\psi_r \tag{6.10}$$

The mesh equations (6.9) und (6.10) describe the so called *T equivalent circuit* shown in the figure 6.2a. After the transition into the Laplace domain the following voltage equations will be obtained for the stationary operation ($s \to j\omega_s$):

$$\mathbf{u}_s = R_s\mathbf{i}_s + j\omega_s\left(L_{s\sigma}\mathbf{i}_s + L_m\mathbf{i}_\mu\right) \tag{6.11}$$

$$0 = \frac{R_r}{s}\mathbf{i}_r + j\omega_s\left(L_{r\sigma}\mathbf{i}_r + L_m\mathbf{i}_\mu\right) \tag{6.12}$$

with the slip $s = \left(\omega_s - \omega\right)/\omega_s$, represented in the figure 6.2b.

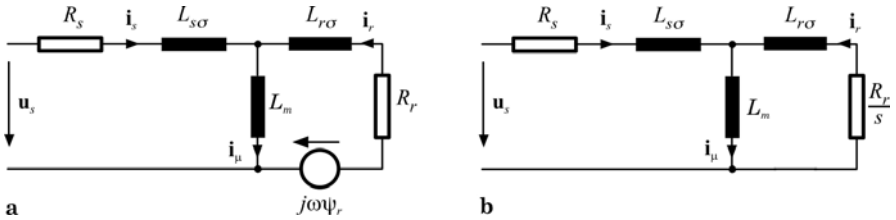

Fig. 6.2 T equivalent circuit of the induction machine: (**a**) non-stationary, (**b**) stationary

With R_s, L_m, $L_{s\sigma}$, $L_{r\sigma}$ and R_r the T equivalent circuit contains five parameters. The stator impedance, determinable by measuring stator quantities, contains on the other hand powers of the stator frequency from zero to three and is defined by four parameters (cf. the chapter 6.4.3). Therefore the T equivalent circuit is over-determined and not completely identifiable by measuring the stator quantities. For this reason $L_{r\sigma} = L_{s\sigma} = L_\sigma$ is often assumed. However, for many tasks it is advisable to change to an equivalent circuit with a reduced parameter number.

The two following representations achieve this by transformation of the leakage inductances into the stator or rotor mesh and by introduction of a total leakage inductance. At the same time this implies a redefinition of the cross or magnetizing current and of the main inductance with the consequence for these quantities losing their physical equivalent. As long as all parameters can be assumed constant and linear, this fact is of minor importance, though. Both new equivalent circuits are derived under the premise that in the case of the squirrel-cage IM no transformation of the stator quantities, measurable at the terminals, takes place.

6.1.1.2 Inverse Γ equivalent circuit

A modified equivalent circuit with the total leakage inductance in the stator mesh can be obtained by the introduction of a new cross current $\mathbf{i}_m$:

$$\mathbf{i}_m = \frac{\psi_r}{L_m} = \mathbf{i}_s + \frac{L_r}{L_m}\mathbf{i}_r \tag{6.13}$$

After some transformations to eliminate the current $\mathbf{i}_\mu$ in equations (6.9), (6.10), and after the introduction of the leakage factor:

$$\sigma = 1 - \frac{L_m^2}{L_s L_r} \tag{6.14}$$

new voltage equations

$$\mathbf{u}_s = R_s \mathbf{i}_s + \sigma L_s \frac{\mathrm{d}\mathbf{i}_s}{\mathrm{d}t} + (1-\sigma) L_s \frac{\mathrm{d}\mathbf{i}_m}{\mathrm{d}t} \tag{6.15}$$

$$0 = \frac{L_m^2}{L_r^2} R_r \left(\frac{L_r}{L_m} \mathbf{i}_r \right) + (1-\sigma) L_s \frac{\mathrm{d}\mathbf{i}_m}{\mathrm{d}t} - j\omega (1-\sigma) L_s \mathbf{i}_m \tag{6.16}$$

which can be represented by the so called inverse-Γ-equivalent circuit (figure 6.3) are obtained. The newly introduced cross current $\mathbf{i}_m$ is according to (6.13) identical with the rotor ampere-turns. This explains why this equivalent circuit is particularly suitable for the treatment of rotor flux orientated control methods. For stationary operation a representation (figure 6.3b) which is equivalent to the figure 6.2b is here possible as well.

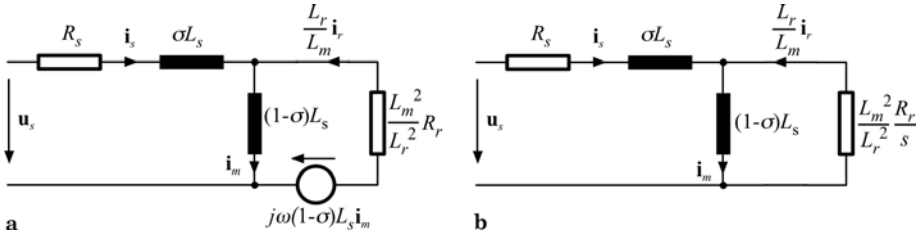

Fig. 6.3 Inverse-Γ-equivalent circuit for the induction machine: (**a**) non-stationary, (**b**) stationary

6.1.1.3 Γ equivalent circuit

To transform the leakage inductance *into the rotor side* a new cross current:

$$\mathbf{i}_{ms} = \frac{\psi_s}{L_s} = \mathbf{i}_s + \frac{L_m}{L_s} \mathbf{i}_r \tag{6.17}$$

is introduced analogously to the inverse Γ equivalent circuit. After substitution of $\mathbf{i}_\mu$ the equations of the Γ equivalent circuit represented in the non-stationary and stationary form in figure 6.4 will be obtained:

$$\mathbf{u}_s = R_s \mathbf{i}_s + L_s \frac{\mathrm{d}\mathbf{i}_{ms}}{\mathrm{d}t} \tag{6.18}$$

$$0 = \frac{L_s^2}{L_m^2} R_r \left(\frac{L_m}{L_s} \mathbf{i}_r \right) + \frac{\sigma L_s}{1-\sigma} \left(\frac{L_m}{L_s} \frac{\mathrm{d}\mathbf{i}_r}{\mathrm{d}t} \right) + L_s \frac{\mathrm{d}\mathbf{i}_{ms}}{\mathrm{d}t} - j\omega \frac{L_s}{L_m} \psi_r \tag{6.19}$$

Also at this place equation (6.14) is valid for the leakage factor σ. The rotor quantities appear, analog to the inverse Γ equivalent circuit, in transformed form.

As recognizable in the figure, the stator inductance now becomes the cross or magnetization inductance, and the stator flux linkage assumes the role of the main flux linkage. Therefore the Γ equivalent circuit is particularly suitable for the treatment of stator flux orientated control methods.

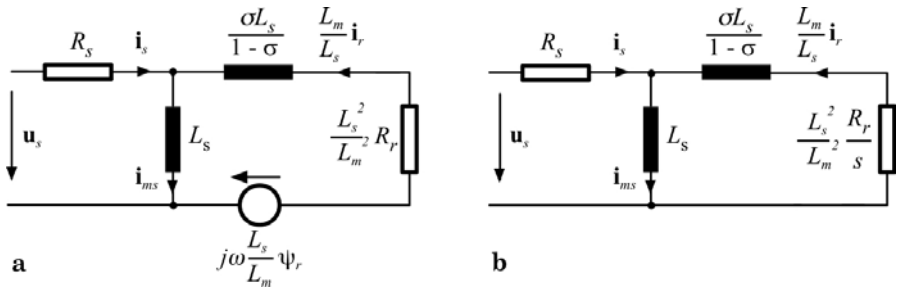

Fig. 6.4 Γ equivalent circuit of the induction machine: (**a**) non-stationary, (**b**) stationary

6.1.2 Equivalent circuits of the PMSM

Due to the permanent magnet excited pole flux the relations here are very simple. To derive a common equivalent circuit for both longitudinal and traverse axes it will usually be accepted that the same inductance is valid for both. The following equation holds for the stator voltage:

$$\mathbf{u}_s = R_s\mathbf{i}_s + L_s\frac{\mathrm{d}\mathbf{i}_s}{\mathrm{d}t} + j\omega\psi_p \tag{6.20}$$

With (6.20) the equivalent circuit represented in the figure 6.5 is obtained.

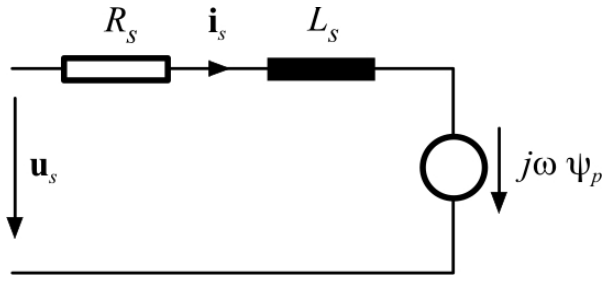

Fig. 6.5 Equivalent circuit of the PMSM

6.2 Modelling of the nonlinearities of the IM

For many control tasks the assumption of constant and state independent machine parameters represents a too rough approximation which leads to considerable deviations between model and reality at the examination of non-stationary operations. Therefore, the embedding of nonlinearities which are significant for different operating states into machine models and equivalent circuits shall be discussed in the following sections. Following the physical conditions, *magnetic saturation, current displacement and iron losses* are discussed in separate approaches and models. Symmetrical conditions and sinusoidal winding distribution are still presupposed.

In mathematical sense nonlinear relations are indicated by the fact that the superposition principle is not valid. Therefore an isolated treatment of the nonlinearities is, strictly speaking, not permitted. With respect to an engineer-like analysis however, it is fundamentally important to find easily comprehensible and utilizable approaches also for nonlinear relations. In the case of the 3-phase AC machines it is advantageous that the most important nonlinearities are describable as state dependent parameters. Since different parameters are affected, or the variable parameters depend on different state variables, a separate treatment is justified additionally.

6.2.1 Iron losses

Losses in the iron appear in the form of eddy-current losses and hysteresis losses. Because the rotor frequency remains small compared with the stator frequency unless at very small speeds, the rotor iron losses generally can be neglected compared to the stator side ones. The hysteresis losses are produced by the flux reversal energy consumed due to the sinusoidal with time varying iron magnetization. They are therefore proportional to the area of the hysteresis loop ($\sim|\psi_\mu|^2$) and to the number of flux reversals per time unit ($\sim\omega_s$) [Lunze 1978], [Philippow 1980]. The eddy-current losses are proportional to the square of the voltage ($\sim(\omega_s|\psi_\mu|)^2$) induced in the iron and the effective electrical conductivity of the iron core lamellae. They significantly increase in converter fed motors because of the harmonic components in current and voltage.

Modeling is made difficult because the effects of eddy-currents and hysteresis and from sinusoidal magnetization are overlapping in a not exactly determinable way, and generally different magnetic conditions occur in yoke and teeth. The hysteresis losses depend on the effective permeability and therefore on the instantaneous flux amplitude. They

disappear as soon as the area of the magnetic saturation is left (the upper field weakening area).

The following, strongly idealized model following [Murata 1990] takes into account hysteresis and eddy-current parts by respectively constant factors k_{hy} and k_w. Through consideration of the slip frequency ω_r even operating states in which the slip frequency will have a significant magnitude compared to the stator frequency ω_s are included:

$$p_{v,fe} = \frac{3}{2}\left[k_{hy}\left(\omega_s + \omega_r\right) + k_w\left(\omega_s^2 + \omega_r^2\right)\right]\left|\,\psi_\mu\right|^2 \tag{6.21}$$

with:

$$\psi_\mu = L_m \mathbf{i}_\mu \tag{6.22}$$

After separating the stator frequency and the slip $s = \left(\omega_s - \omega\right)/\omega_s$, and with the general equation for the iron losses

$$p_{v,fe} = \frac{3}{2}\frac{\left(\omega_s\left|\psi_\mu\right|\right)^2}{R_{fe}} \tag{6.23}$$

an iron loss resistance R_{fe} as concentrated component describing the iron losses can be introduced:

$$R_{fe} = \frac{1}{k_w\left(1+s^2\right) + \dfrac{k_{hy}}{\omega_s}\left(1+s\right)} \tag{6.24}$$

Because better usability in some circumstances the iron loss conductance $G_{fe} = 1/R_{fe}$ is also used. A measured R_{fe} characteristics is represented exemplarily in the figure 6.6. The curves are the result of no-load measurements at an inverter-fed and external driven motor so that the influence of the friction losses is eliminated.

The iron loss power is dominated by the hysteresis losses rising nearly linearly in the basic speed range. With field weakening setting in, at first a strong drop can be observed because of the flux reduction. The eddy-current losses dominate in the upper field-weakening area. In addition, the inverter dependent eddy-current losses decrease strongly at the maximum voltage (= less high-frequency voltage harmonics) so that different factors k_w are used in constant flux area and constant voltage range. The corresponding diagrams calculated by least-square approximation and the model approach (6.24) are drawn in the figure 6.6 (dotted lines). It turns out that this simple approach with the above-mentioned modification describes the actual behavior quite well.

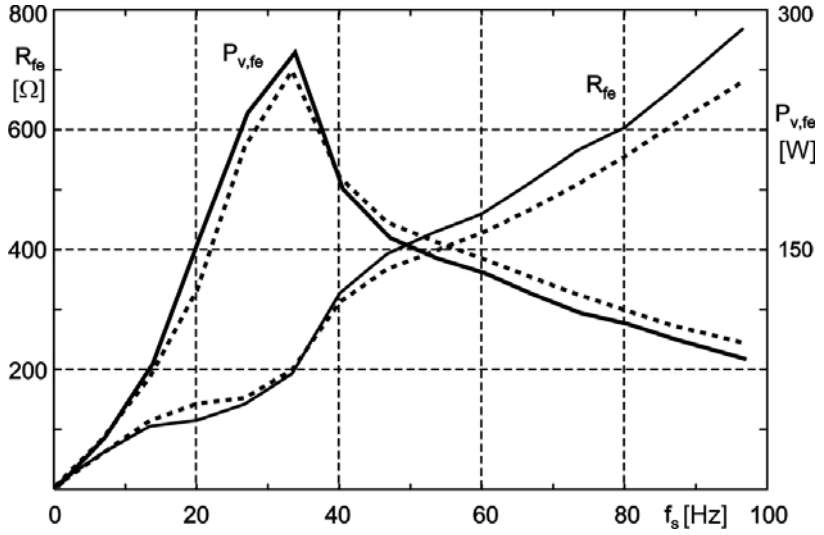

Fig. 6.6 Iron losses and iron loss resistance

Further analysis of the R_{fe}-diagram in the figure 6.6 suggests, however, the possibility of using a yet more simplified model which only contains a linear relation between loss resistance and stator frequency:

$$R_{fe} = R_{feN} \frac{\omega_s}{\omega_{sN}} \tag{6.25}$$

For this model only one parameter, the loss resistance at nominal frequency, must be determined by measurement.

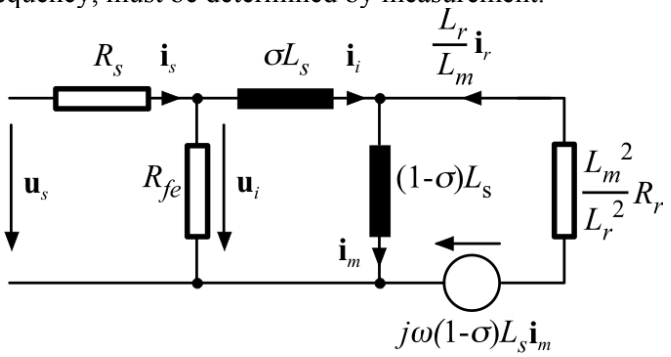

Fig. 6.7 Extended inverse Γ equivalent circuit with iron losses

A comfortable inclusion in the equation system of the IM will be obtained, if (as shown in the figure 6.7) the iron loss resistance in the inverse Γ equivalent circuit can be represented by a parallel resistance in the stator circuit [Schäfer 1989]. The necessary supplementation of the

equation system is immediately recognisable from the figure 6.7. The actual input voltage of the machine will now be formed by the inner voltage $\mathbf{u}_i$ which drives the inner current $\mathbf{i}_i$. Following equations (6.15) and (6.16) the modified system is obtained to:

$$\mathbf{u}_i = \sigma L_s \frac{\mathrm{d}\,\mathbf{i}_i}{\mathrm{d}\,t} + (1-\sigma) L_s \frac{\mathrm{d}\,\mathbf{i}_m}{\mathrm{d}\,t} \tag{6.26}$$

$$0 = (1 - j\omega T_r)\mathbf{i}_m + T_r \frac{\mathrm{d}\,\mathbf{i}_m}{\mathrm{d}\,t} - \mathbf{i}_i \tag{6.27}$$

$$\mathbf{u}_i = \mathbf{u}_s - R_s \mathbf{i}_s \tag{6.28}$$

$$\mathbf{i}_i = \mathbf{i}_s - \frac{\mathbf{u}_i}{R_{fe}} \tag{6.29}$$

6.2.2 Current and field displacement

With regard to current and field displacement effects it must be distinguished between effects caused by the fundamental of the current on one hand and by inverter dependent current harmonics on the other hand. The principle physical mechanism is the same in both cases. The current displacement leads to a frequency dependent increase of the resistance values, and the field displacement to a reduction of the leakage inductances. As a consequence the current harmonics produce higher losses. Because the harmonic spectrum of fast switching inverters with sine modulation is orders of magnitude above the fundamental wave, its significance for control related parameters remains small. The consequences of the fundamental dependent current displacement, however, must be investigated for the modeling of the machine.

In stator windings of induction machines, fundamental wave dependent current displacement effects can usually be neglected since they are intentionally suppressed by a number of constructive measures. An exception would merely be the big machines with accordingly large winding diameters at high frequencies. For the bars of the rotor squirrel-cage such a neglection is not possible from the outset because of the large bar heights and diameters, except for rotors with intentionally current displacement free construction. In the normal (stationary) operation current displacement effects do not play a considerable role, however, because of the low rotor frequency (slip). This turns different in special non-stationary operation modes with high slip frequencies, where the current displacement is used with purpose to increase the resistance, or if the input quantities are controlled differently to the normal operation. In a field-orientated control system however, also at start-up extreme slip values will

not appear due to the current being controlled with defined amplitude and slip.

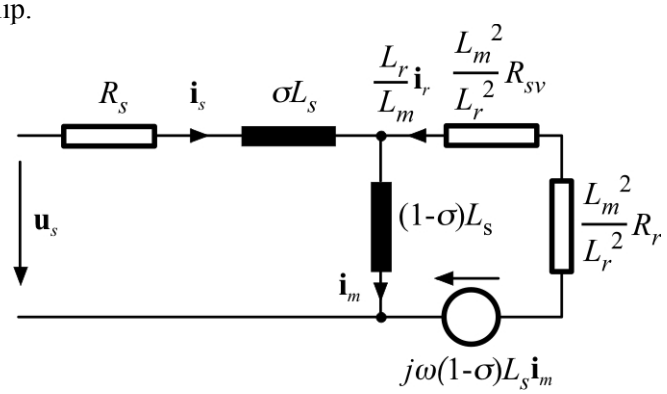

Fig. 6.8 Extended equivalent circuit with current displacement in rotor

A consideration of the resistance changes in the machine model is possible by an additional resistance R_{sv} being inserted in series to the rotor resistance in the rotor circuit (figure 6.8). The size of this resistance is a generally very unhandy function of material constants, construction data and the rotor frequency. The following equation can be learned from [Vogt 1986] for a rectangular deep-bar rotor with the height h_l:

$$k_r = \frac{R_r + R_{sv}}{R_r} = \beta \frac{\sinh 2\beta + \sin 2\beta}{\cosh 2\beta - \cos 2\beta} \tag{6.30}$$

There β is a normalized height of the conductor and is calculated by:

$$\beta = h_l \sqrt{\frac{1}{2}\omega_r \mu_0 \kappa} \tag{6.31}$$

μ_0 Absolute permeability
κ Conductivity of rotor bars

Because the height of rotor bars is often designed over-critically (rotor with current displacement), h_l assumes values of up to about 70 mm. Following [Vogt 1986] this corresponds to a machine with a rated power of about 2 MW. Therefore it is not possible to come up with a uniform approximation for k_r for the complete interesting parameter range of β. The following variants for approximation approaches can be derived:

For $\beta > 2$ there will be $\sinh\beta >> \sin\beta$, $\cosh\beta >> \cos\beta$ and $\sinh\beta \approx \cosh\beta$, and therefore holds:

$$k_r \approx \beta \tag{6.32}$$

For $\beta \leq 2$, k_r can be obtained by series expansion of the transcendental function with a maximum relative fault of 0.036 to:

$$k_r \approx \frac{1+\frac{2}{15}\beta^4}{1+\frac{2}{45}\beta^4} \tag{6.33}$$

A next approximation is possible for $\beta \leq 1$ by partial division of (6.33):

$$k_r \approx 1+\frac{4}{45}\beta^4 \tag{6.34}$$

Besides the increase of the electrical resistance by current displacement, fast changes of the flux will cause a field displacement recognized by the reduction of the leakage inductance. Also here, noticeable effects appear only in rotors with current displacement because of the larger conductor height. A reduction factor k can be given in analogy to (6.30). Following [Vogt 1986] this factor can be written for square deep-bar rotors with the fictitious series inductance $L_{\sigma v}$ to:

$$k_x = \frac{L_\sigma - L_{\sigma v}}{L_\sigma} = \frac{3(\sinh 2\beta - \sin 2\beta)}{2\beta(\cosh 2\beta - \cos 2\beta)} \tag{6.35}$$

As above the following approximations can be derived.

- For $\beta > 2$:

$$k_x \approx \frac{3}{2\beta} \tag{6.36}$$

- For $1 < \beta \leq 2$:

$$k_x \approx \frac{1+\frac{2}{105}\beta^4}{1+\frac{2}{45}\beta^4} \tag{6.37}$$

- For $\beta \leq 1$:

$$k_x \approx 1-\frac{8}{315}\beta^4 \tag{6.38}$$

The equations (6.30) and (6.35) are represented in figure 6.9. For the better classification the normalized bar height β is additionally referred to the rotor frequency at different absolute bar heights. The computation was made for copper bars because these also have greater values β due to their greater conductivity compared with aluminum at the same frequency.

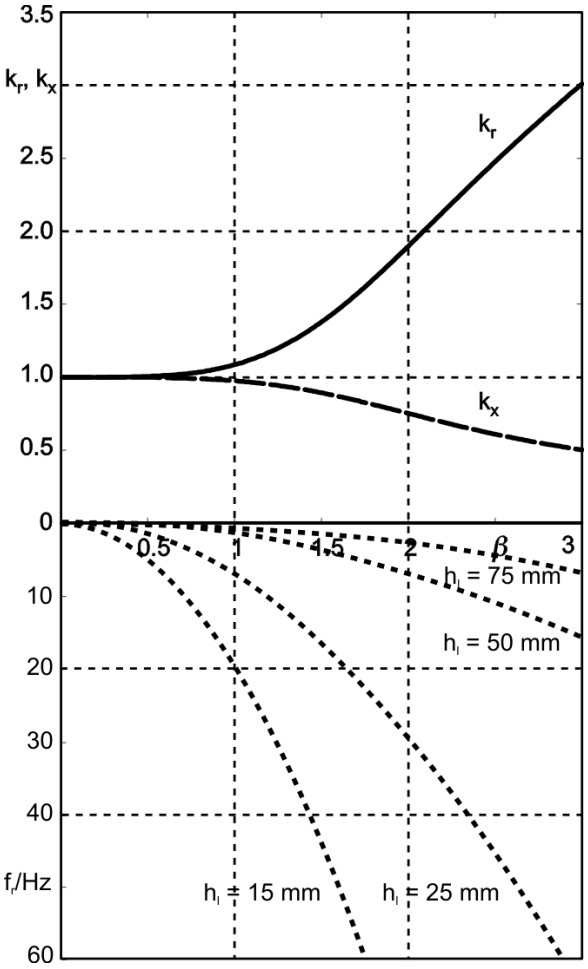

Fig. 6.9 Electrical resistance increase (___) and leakage inductance reduction (**.....**) due to current displacement in the rotor, parameter: bar height and rotor frequency

For very big machines in the megawatt range β already reaches great values at rotor frequencies below 10 Hz, and k_r and k_x also become significant. Such machines have a small nominal slip of typical below one hertz, and will be less overloaded in dynamic operation, though. In low power drive systems, only three to four times the nominal slip will be applied in dynamic operation using *field-orientated control*. Thus β will not exceed values of 1.5 through the whole power range, and for motors in the medium and low power range there are values of $\beta = 1$ to be expected at maximum. Because the rotor leakage inductance only shares about one

half of the total leakage inductance, a special consideration of the inductance reduction can be abandoned in the model for field-orientated control. A consideration of the electrical resistance increase in the model for the field-orientated control is required only for machines above some hundred kilowatts rating.

The existence of the flux weakening and resistance increase must be taken into account though at the estimation of parameter variations or for example to define suitable excitation signals for the parameter identification especially at higher frequencies (cf. section 6.4).

The structure of the equations (6.30) and (6.35) is essentially correct also for usual bar cross-sections which differ from the rectangle form, though with other coefficients. Approximately the same relations hold for square bars with $d = h_l$ and for rods (diameter d). For wedge bars the value k_r increases in the extreme case (ratio of the trapezium front sides of 1:10) at $\beta = 2$ by 50 %. k_x assumes more favourable values [Vogt 1986]. Thus the above statements remain also valid for these bar forms.

6.2.3 Magnetic saturation

At first the magnetic saturation has the consequence that the value of the inductances is a nonlinear function of the amplitude of the actual flux linkage. In addition, a general analysis of the saturated induction machine must take into account that the spatial distribution of the saturation depends on the current direction of the accompanying flux vector. This has the consequence that in the right-angled coordinate system the inductances assigned to the coordinate axes assume different values in the dynamic case, and mutual couplings appear [Vas 1990]. These depend on the sine of the angle between the main flux vector and the reference axis (real axis) of the used coordinate system.

The main field saturation has essential significance for the dynamic behavior of the machine, primarily in the field weakening and at great torques. Its correct or reasonable approximated consideration shall be examined in the following. At first the leakage inductances are considered as constant.

For a representation as generally as possible the machine equations are represented in the following in a right-angled coordinate system circulating with the angular velocity ω_k. The main flux linkage

$$\psi_\mu = L_m \mathbf{i}_\mu \tag{6.39}$$

is introduced into the general voltage equations of the induction machine (cf. section 3.2). With (6.39) the following voltage equations will be obtained:

$$\mathbf{u}_s = R_s\mathbf{i}_s + L_{s\sigma}\frac{\mathrm{d}\mathbf{i}_s}{\mathrm{d}t} + \frac{\mathrm{d}\psi_\mu}{\mathrm{d}t} + j\omega_k(L_{s\sigma}\mathbf{i}_s + L_m\mathbf{i}_\mu) \tag{6.40}$$

$$\mathbf{u}_r = R_r(\mathbf{i}_\mu - \mathbf{i}_s) + L_{r\sigma}\frac{\mathrm{d}(\mathbf{i}_\mu - \mathbf{i}_s)}{\mathrm{d}t} + \frac{\mathrm{d}\psi_\mu}{\mathrm{d}t} + j(\omega_k - \omega)(L_r\mathbf{i}_\mu - L_{r\sigma}\mathbf{i}_s) \tag{6.41}$$

The equations (6.40) and (6.41) are here still represented in an arbitrary orientated coordinate system and contain no restrictions regarding their validity at main field saturation. Following [Vas 1990] the next equation holds for the derivative of the main flux:

$$\frac{\mathrm{d}\psi_\mu}{\mathrm{d}t} = \begin{pmatrix} M_x & M_{xy} \\ M_{xy} & M_y \end{pmatrix}\frac{\mathrm{d}\mathbf{i}_\mu}{\mathrm{d}t} \tag{6.42}$$

with: $M_x = L_m' \cos^2\mu + L_m \sin^2\mu$

$M_y = L_m' \sin^2\mu + L_m \cos^2\mu$

$M_{xy} = (L_m' - L_m)\sin\mu\cos\mu$

Thereby $L_m(|\mathbf{i}_\mu|)$ is the static and $L_m'(|\mathbf{i}_\mu|) = \frac{\mathrm{d}|\psi_\mu|}{\mathrm{d}|\mathbf{i}_\mu|} = L_m + \frac{\mathrm{d}L_m}{\mathrm{d}|\mathbf{i}_\mu|}|\mathbf{i}_\mu|$ the differential main inductance, μ is the angle between the magnetizing current vector $\mathbf{i}_\mu$ and the real axis of the coordinate system. For the non-saturated machine $L_m = L_m'$ and $\frac{\mathrm{d}\psi_\mu}{\mathrm{d}t} = L_m\frac{\mathrm{d}\mathbf{i}_\mu}{\mathrm{d}t}$ hold.

For the controller realization and also for a simulation of the saturated machine the correct representation of the flux derivation following (6.42) is quite unhandy. For the controller design primarily the rotor equation is important because the estimation equation of the rotor flux, required for field-orientated control, is derived from it. Therefore it would be desirable to maintain the rotor flux oriented description.

A first simplification (without validity restriction or loss of precision) arises with representation of (6.40) and (6.41) in a coordinate system related to the main flux. If the axis of the main flux vector and the real axis (x-axis) are identical, it will be $\mu = 0$, and the next equation can be obtained for the flux derivative:

$$\frac{\mathrm{d}\psi_\mu}{\mathrm{d}t} = \begin{pmatrix} L_m'(|\mathbf{i}_\mu|) & 0 \\ 0 & L_m(|\mathbf{i}_\mu|) \end{pmatrix}\frac{\mathrm{d}\mathbf{i}_\mu}{\mathrm{d}t} \tag{6.43}$$

In addition, there are $\psi_{\mu x} = |\psi_\mu|$ and $\psi_{\mu y} = 0$.

Since obviously the flux derivative is the most problematic part of the mathematical model, it seems reasonable to look for a form of presentation which gets along without its explicit calculation. In addition, no derivative of a state variable must be connected with the main inductance. Such a model was developed in [Levi 1994]. The rotor current is replaced by the flux linkage in the rotor voltage equation:

$$\mathbf{u}_r = \dot{\boldsymbol{\psi}}_\mathrm{r} + j\left(\omega_k - \omega\right)\boldsymbol{\psi}_r + \frac{R_r}{L_{r\sigma}}(\boldsymbol{\psi}_r - \boldsymbol{\psi}_\mu) \tag{6.44}$$

The mutual flux can be calculated from:

$$\boldsymbol{\psi}_\mu = \boldsymbol{\psi}_r - L_{r\sigma}(\mathbf{i}_\mu - \mathbf{i}_s) \tag{6.45}$$

with: $$\mathbf{i}_\mu = \frac{\boldsymbol{\psi}_\mu}{L_m(|\boldsymbol{\psi}_\mu|)}$$

It shall be remarked that this model also does not contain any restrictions regarding the saturation and is neutrally formulated with respect to coordinates. The calculation of a differential inductance is not required. As opposed to (6.41), the equation (6.45) contains with $\boldsymbol{\psi}_\mu = f(L_m(|\boldsymbol{\psi}_\mu|))$ an algebraic loop which can cause oscillations and limit cycles depending on the sampling period or on the integration steps in the realization.

A third model can be obtained after trying to introduce the saturation into the rotor equation immediately without further substitutions. This means, though, that the saturation is coupled to the rotor flux instead to the main flux, what does not correspond to the physical conditions correctly. The error can, however, be acceptable for many applications because the leakage flux on the rotor side will always remain small compared to the main flux. In any case this variant has the advantage to provide the simplest and clearest model. A possibility for its derivation immediately arises from the equivalent circuit in figure 6.3a. After substitution of the rotor current and division by the leakage factor $(1-\sigma)$, which shall be assumed as saturation invariant, the following equation for the rotor mesh can be obtained after transition into the coordinate system circulating with ω_k:

$$\mathbf{u}_r = R_r(\mathbf{i}_m - \mathbf{i}_s) + \frac{\mathrm{d}(L_s\mathbf{i}_m)}{\mathrm{d}t} + j\left(\omega_k - \omega\right)L_s\mathbf{i}_m \tag{6.46}$$

After dissolving the derivative, the rotor equation can finally be written in a detailed notation:

$$\mathbf{u}_r = \mathbf{i}_m - \mathbf{i}_s + \frac{L_m'(|\mathbf{i}_m|) + L_\sigma}{R_r}\frac{\mathrm{d}\,\mathbf{i}_m}{\mathrm{d}\,t} + j\left(\omega_k - \omega\right)\frac{L_m(|\mathbf{i}_m|) + L_\sigma}{R_r}\mathbf{i}_m \tag{6.47}$$

In the same way the stator voltage equation can be obtained for an assumed constant leakage inductance:

$$\mathbf{u}_s = R_s\mathbf{i}_s + \sigma L_s\frac{\mathrm{d}\,\mathbf{i}_s}{\mathrm{d}\,t} + j\omega_k\sigma L_s\mathbf{i}_s + (1-\sigma)\left(L_m'(|\mathbf{i}_m|) + L_\sigma\right)\frac{\mathrm{d}\,\mathbf{i}_m}{\mathrm{d}\,t} + j\omega_k(1-\sigma)\left(L_m(|\mathbf{i}_m|) + L_\sigma\right)\mathbf{i}_m \tag{6.48}$$

The modified system matrix of the continuous state-space representation finally can be derived from (6.47) and (6.48). It reads in complex notation with the abbreviations $L_{s\mu} = L_m\left(|\mathbf{i}_m|\right) + L_\sigma$ and $L_{s\mu}' = L_m'\left(|\mathbf{i}_m|\right) + L_\sigma$:

$$\mathbf{A} = \begin{pmatrix} -\frac{1}{T_\sigma} - j\omega_k & \frac{1-\sigma}{\sigma L_s}\left(R_r - j\omega L_{s\mu}\right) \\ \frac{R_r}{L_{s\mu}'} & -\frac{R_r}{L_{s\mu}'} - j\left(\omega_k - \omega\right)\frac{L_{s\mu}}{L_{s\mu}'} \end{pmatrix} \tag{6.49}$$

with: $T_\sigma = \dfrac{\sigma L_s}{R_s + (1-\sigma)R_r}$

At first the model (6.47) yields the rotor-side magnetizing current $\mathbf{i}_m$. The rotor flux linkage can be calculated from $\psi_r = L_m\mathbf{i}_m$. For this calculation the main inductance has to be used depending on the magnetizing current $\mathbf{i}_\mu$. With (6.8) and (6.4) its amplitude can be derived in the rotor flux orientated coordinate system ($\mathbf{i}_m = i_{md}$, $i_{mq} = 0$):

$$\left|\mathbf{i}_\mu\right| = \sqrt{\left(\frac{L_{r\sigma}}{L_r}i_{sd} + \frac{L_m}{L_r}i_{md}\right)^2 + \left(\frac{L_{r\sigma}}{L_r}i_{sq}\right)^2} \tag{6.50}$$

For the stationary case the following result arises:

$$\left|\mathbf{i}_\mu\right| = \sqrt{i_{md}^2 + \left(\frac{L_{r\sigma}}{L_r}i_{sq}\right)^2} \tag{6.51}$$

The knowledge of the magnetization characteristic, either in the form $\psi_\mu = f(\mathbf{i}_\mu)$ or its inverse form $\mathbf{i}_\mu = g(\psi_\mu)$, is required for all saturation dependent models. Thereby the use of a closed representation is advisable,

because this can more simply be implemented in the model and simultaneously allows the calculation of the differential inductance without difficulties from the measurement of the stationary characteristic. In the literature different approaches can be found, which are based on exponential or power functions and differ from each other in the number of contained parameters. Polynomial approaches are also used. Exponential and power functions have the advantage to provide good models even at strong saturation. Two power functions, which are built on each other, shall be examined and compared in the following. They are based on a approach introduced by [de Jong 1980] and further developed by [Klaes 1992].

The main inductance is understood as a parallel circuit of a constant air-gap inductance L_0 (it corresponds to the main inductance in the linear range) and a saturation dependent part which is a power function of the obtained main flux or magnetizing current:

$$L_m(\gamma) = \frac{1}{\frac{1}{L_0} + \frac{\gamma^s}{L_{sat}}}; \gamma = \frac{i_\mu}{i_1} \tag{6.52}$$

With measured values $L_0 = L_m(0), L_1 = L_m(1), L_2 = L_m(\gamma_2)$ the remaining parameters are obtained as follows:

$$L_{sat} = \frac{1}{\frac{1}{L_1} - \frac{1}{L_0}}; s = \frac{\ln\left(\frac{1/L_2 - 1/L_0}{1/L_1 - 1/L_0}\right)}{\ln \gamma_2} \tag{6.53}$$

An extended approach takes into account, that the main inductance converges towards a fixed final value and not towards zero for large flux amplitudes, as it would result from the estimation function (6.52). This is considered by the addition of a limit inductance L_∞ into (6.52):

$$L_m(\gamma) = \frac{1}{\frac{1}{L_0 - L_\infty} + \frac{\gamma^s}{L_{sat}}} + L_\infty \tag{6.54}$$

For the calculation of the coefficients however, no explicit solution can be derived. With the additional measurement $L_3 = L_m(\gamma_3)$ the saturation parameter *s* arises from the iterative solution of the following equation:

$$\left(\frac{\gamma_1}{\gamma_2}\right)^s - \frac{(L_2 - L_3)(L_1 - L_0) + (L_2 - L_1)(L_0 - L_3)\left(\frac{\gamma_1}{\gamma_3}\right)^s}{(L_3 - L_1)(L_0 - L_2)} = 0 \tag{6.55}$$

For the remaining parameters the next equations hold:

$$L_\infty = \frac{L_3(L_1 - L_0) + L_1(L_0 - L_3)\left(\frac{\gamma_1}{\gamma_3}\right)^s}{L_1 - L_0 + (L_0 - L_3)\left(\frac{\gamma_1}{\gamma_3}\right)^s} \tag{6.56}$$

$$\frac{1}{L_{sat}} = \frac{1}{\gamma_2^s - \gamma_3^s}\left(\frac{1}{L_2 - L_\infty} - \frac{1}{L_3 - L_\infty}\right) \tag{6.57}$$

The estimates are represented together with the characteristic for the differential main inductance for an 11kW motor in figure 6.10. The differential main inductance can be calculated for the three-parameter approach from:

$$L_m'(\gamma) = \frac{\mathrm{d}\psi_\mu}{\mathrm{d}i_\mu} = L_m(\gamma)\left(1 - s\gamma^s \frac{L_m(\gamma)}{L_{sat}}\right) \tag{6.58}$$

and for the four-parameter approach from:

$$L_m'(\gamma) = L_m(\gamma) - s\gamma^s \frac{(L_m(\gamma) - L_\infty)^2}{L_{sat}} \tag{6.59}$$

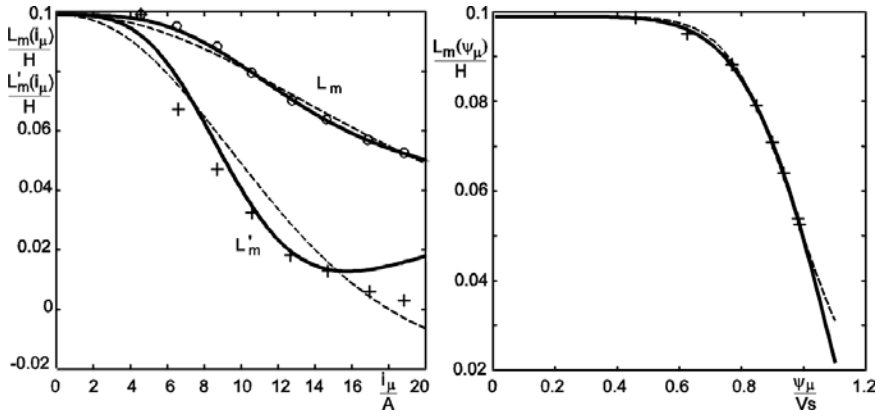

Fig. 6.10 Saturation calculation functions $L_m\left(i_\mu\right), L_m'\left(i_\mu\right), L_m\left(\psi_\mu\right)$ for 11kW motor. (----): three-parameter model; (——): four-parameter model

The measurements of the static inductance are visibly better approximated by the four-parameter approach. Apart from the area of extreme saturation, which practically plays not a role, this also applies to the differential inductance. It must be taken into account that the

"measured values" of the differential inductance only were won by linear approximation from the static measurements, though.

The saturation of the leakage paths is the reason that the leakage inductances generally are functions of the current flowing through them. A general relation like for the main inductance however, can not be derived because it depends strongly on constructive influences according to the composition of the leakage field (slot leakage, tooth head leakage, winding head leakage, helical leakage). At the same time it is possible that almost no current dependency of the leakage inductance can be found for many motors in the complete current range. For this reason, a separate consideration in the model is abandoned. If required, a feed-forward adaptation $L_\sigma = f(|\mathbf{i}_s|)$ must be implemented.

6.2.4 Transient parameters

When discussing the current displacement effects it already became obvious that inductances and resistances of the induction machine generally have to be considered frequency dependent. Equivalent circuits can be developed with concentrated parameters which, however, have to be specified according to the operating point of interest and to the operation frequency. In an inverter-fed drive the highest frequencies practically appearing are determined by the switching slopes of the inverter. These have an effect on the effective leakage inductance of the motor which determines together with the voltage amplitude the current rise time. The effective leakage inductance is to be expected considerably smaller than the stationary leakage inductance σL_s and will be called in the following as the transient leakage inductance $\sigma L_s'$. At the same time it is the only parameter which must especially be defined in the practical controller design for transient operations.

6.3 Parameter estimation from name plate data

Lacking detailed and often not obtainable motor data sheets, the name plate of the motor represents the first and only information source for conclusions on the electrical parameters. For standard drives without high dynamic demands on the motor usage, usually it fully suffices to calculate the motor parameters from the name plate data. However, deviations from 50% to 100% depending on the parameter in question have to be taken into account, because:

- the manufacturer's information may be partly unreliable, and the actual motor parameters are subject to spreads,
- the name plate data refer to a certain working point (the nominal working point),
- not all parameters of the equivalent circuit can be directly set into a physical relation to the usual name plate data.

The procedure becomes impossible at the use of special machines with values differing from standard machines considerably. Understandably, the calculation of the inductance saturation characteristic has to be excluded.

The usual name plate data are:

- Nominal power P_N [kW]
- (Line-to-line) nominal voltage U_N [V]
- Nominal current I_N [A]
- Nominal frequency f_N [Hz]
- Nominal speed n_N [rpm]
- (Nominal) power factor $\cos\varphi$

Because the last information is not available in many cases, calculation equations are derived in the following without and with $\cos\varphi$. In the case PMSM, the following data are usually given by the name plate:

- (Line-to-line) nominal voltage U_N [V / 1000 rpm]
- Nominal current I_N [A]
- Nominal frequency f_N [Hz]
- Maximum speed n_{max} [rpm]
- Nominal torque m_N [Nm]

6.3.1 Calculation for IM with power factor cosφ

The method starts out from the equation of the IM in the stationary operation (cf. [Quang 1996]).

$$\begin{aligned}\mathbf{u}_s &= R_s\,\mathbf{i}_s + j\omega_s\sigma L_s\mathbf{i}_s + j\omega_s\left(1-\sigma\right)L_s\frac{\psi_r}{L_m}\\ &= R_s\,\mathbf{i}_s + j\omega_s\sigma L_s\mathbf{i}_s + \mathbf{e}_g\end{aligned} \tag{6.60}$$

The parameters are approximately calculated for the nominal working point in the following steps:

1. *Calculation of the field-forming current component i_{sd}:*

   (1) Nominal power of the motor: $P_N = 3U_{Phase}I_{Phase}\cos\varphi$

   (2) Amplitude of the nominal current: $\hat{I}_N = \sqrt{2}\,I_N = \sqrt{\hat{I}_{sdN}^2 + \hat{I}_{sqN}^2}$

   (3) Impedance of one phase: $Z_N = U_{Phase}/I_{Phase}$

(4) Approximate rotor resistance: $R_r \approx s Z_N$

(5) Nominal power of the motor: $P_N \approx 3\left(\frac{R_r}{s}\right)\hat{I}_{sqN}^2$

(6) From (4), (5) is obtained: $\hat{I}_{sqN}^2 \approx \frac{P_N}{3Z_N}$

(7) Inserting (1) into (6): $\hat{I}_{sqN}^2 \approx \frac{U_{Phase} I_{Phase} \cos\varphi}{Z_N}$

(8) Inserting (7) into (2): $\hat{I}_{sdN} \approx \sqrt{\hat{I}_N^2 - \frac{U_{Phase} I_{Phase} \cos\varphi}{Z_N}}$

The following approximate formula can be derived from (8):

$$\hat{I}_{sdN} \approx \sqrt{2} I_N \sqrt{1-\cos\varphi} \tag{6.61}$$

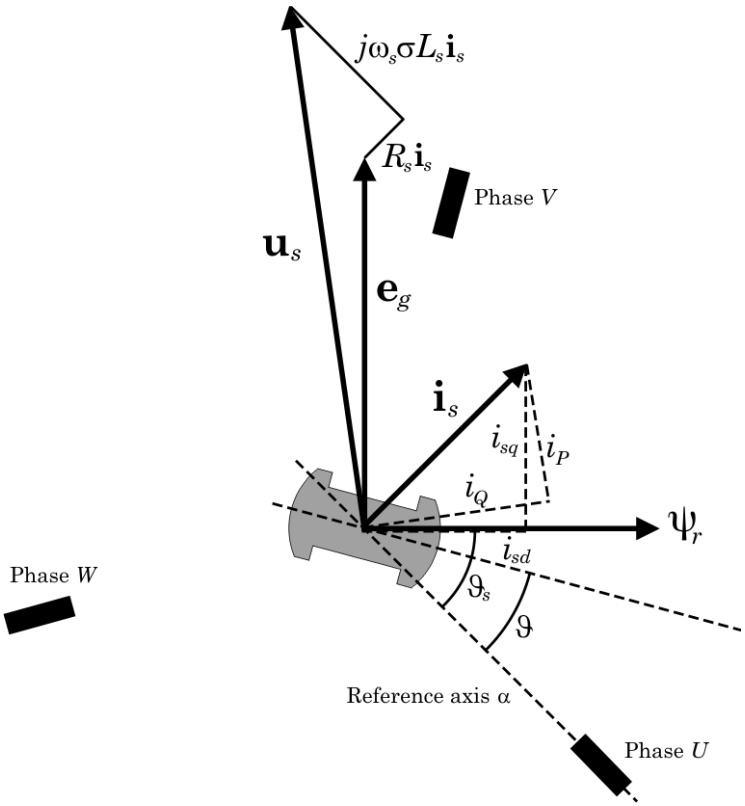

Fig. 6.11 Vector diagram of the IM in the stationary operation

In the step (5) the losses in the stator resistance were neglected without great loss of precision for the calculation of the power P_N.

2. *Calculation of the torque-forming current component* i_{sq}

$$\hat{I}_{sqN} \approx \sqrt{2I_N^2 - \hat{I}_{sdN}^2} \tag{6.62}$$

3. *Calculation of* ω_r

$$\omega_{rN} = 2\pi\left(f_N - \frac{z_p\, n_N}{60}\right) \tag{6.63}$$

4. *Calculation of the rotor time constant* T_r

$$T_r = \frac{\hat{I}_{sqN}}{\omega_{rN}\,\hat{I}_{sdN}} \tag{6.64}$$

5. *Calculation of the leakage reactance* $X_\sigma = \omega_s \sigma L_s$

The voltage drop over the stator resistance is neglected, which is justified for the nominal working point, compared to the voltage drop over the leakage inductance in the vector diagram in the figure 6.11. The simplified vector diagram of the figure 6.12 can be obtained then.

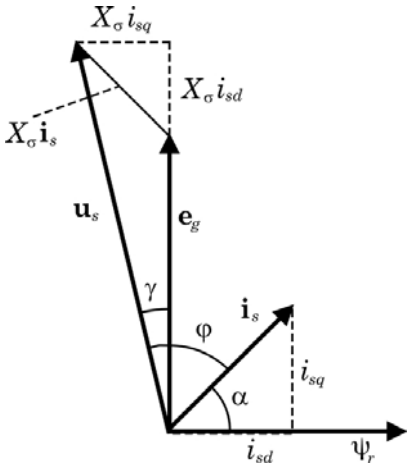

Fig. 6.12 Simplified vector diagram for calculation of X_σ

Using the figure 6.12 the following calculation steps can be used:

(1) Amplitude of the nominal phase voltage: $\hat{U}_N = \frac{\sqrt{2}\,U_N}{\sqrt{3}}$

(2) Relations between α, $\hat{I}_{sdN}$ and $\hat{I}_{sqN}$: $\sin\alpha = \frac{\hat{I}_{sqN}}{\hat{I}_N}; \cos\alpha = \frac{\hat{I}_{sdN}}{\hat{I}_N}$

(3) Relation between α, γ and φ: $\gamma = \varphi - \left(90^0 - \alpha\right)$

(4) Calculation of $\sin\gamma$:

$$\begin{aligned}\sin\gamma &= \sin\left[\varphi - \left(90^0 - \alpha\right)\right] \\ &= \sin\varphi\,\sin\alpha - \cos\varphi\,\cos\alpha\end{aligned}$$

(5) Inserting (2) into (4): $\sin\gamma = \sin\varphi\frac{\hat{I}_{sqN}}{\hat{I}_N} - \cos\varphi\frac{\hat{I}_{sdN}}{\hat{I}_N}$

(6) From fig. 6.12 it will be obtained: $X_\sigma \approx \sin\gamma\frac{\widehat{U}_N}{\hat{I}_{sqN}}$

(7) Inserting (5) into (6): $X_\sigma \approx \left(\sin\varphi - \cos\varphi\frac{\hat{I}_{sdN}}{\hat{I}_{sqN}}\right)\frac{\widehat{U}_N}{\hat{I}_N}$

With these results the formula for the calculation of X_σ is obtained:

$$X_\sigma \approx \left(\sin\varphi - \cos\varphi\frac{\hat{I}_{sdN}}{\hat{I}_{sqN}}\right)\frac{U_N}{\sqrt{3}\,I_N} \tag{6.65}$$

6. *Calculation of the main reactance X_h:*

The main reactance $X_h = \omega_s(1-\sigma)L_s \approx \omega_s L_s$ is the reactance of the EMF e_g. In the case i_{sq} = 0, i.e. no-load, the calculation equation is approximately obtained from the figure 6.12:

$$X_h \approx \frac{\widehat{U}_N}{\hat{I}_{sdN}} - X_\sigma = \frac{\sqrt{2}\,U_N}{\sqrt{3}\,\hat{I}_{sdN}} - X_\sigma \tag{6.66}$$

7. *Calculation of the stator resistance R_s:*

(1) It is assumed approximately: $R_s \approx R_r$

(2) Calculation of the EMF amplitude: $\hat{\mathbf{e}}_\mathbf{g} = X_h\hat{I}_{sdN} \approx \frac{R_r}{\omega_{rN}/(2\pi f_N)}\hat{I}_{sqN}$

The definite formula then looks as follows:

$$R_s \approx R_r \approx \frac{\omega_{rN}}{2\pi f_N}\frac{\hat{I}_{sdN}}{\hat{I}_{sqN}}X_h \tag{6.67}$$

8. *Calculation of the total leakage factor σ:*

$$\sigma \approx \frac{X_\sigma}{X_h} \tag{6.68}$$

9. *Calculation of the stator-side time constant T_s:*

$$T_s = \frac{L_s}{R_s} \approx \frac{X_h}{2\pi f_N R_s} \tag{6.69}$$

The given calculation with using cosφ was tested successfully in the practice and is not subject to any restriction regarding motor power.

6.3.2 Calculation for IM without power factor cosφ

Reference model is the inverse Γ equivalent circuit of the IM. All formulae are valid for motors with a nominal power of greater than 0.7kW.

The total leakage reactance determines fundamentally the short circuit behaviour of the motor or the current amplitude at nominal frequency at turn-on to the stiff grid. For standard motors the turn-on current maximum is 4 to 7 times the nominal current. Empirical values show that the most correct values for the leakage inductance σL_s will be obtained, if the 5 to 6-fold nominal current is used:

$$\sigma L_s \approx \frac{U_N}{5.5 I_N \omega_N \sqrt{3}} \tag{6.70}$$

For the transient leakage inductance a value of about $0.8\sigma L_s$ can be started with.

The stator reactance is responsible for the current consumption of the no-load machine. This depends for comparable power ratings strongly on the magnetic utilization of the machine, thus on the nominal working point regarding the magnetic saturation, and therefore it can be subject to considerable variations for different manufacturers. Without using the power factor we can start out from the approximate rule that the nominal no-load current I_0 is about half of the nominal current at small power (until 7.5kW) and tends above this power towards to a good third of the nominal current. The following formula represents this empirical value:

$$I_0 \approx \frac{I_N + 1.9A}{2.6} \tag{6.71}$$

$$L_s = \frac{U_N}{I_0 \omega_N \sqrt{3}} \tag{6.72}$$

No physical relations can be given for the calculation of the stator resistance from the nominal data. We are here completely dependent on empirical values with the unavoidable uncertainties. The following formula provides usable results:

$$R_s \approx \frac{0.02\, U_N}{I_N - 2.0\, A} \tag{6.73}$$

The rotor resistance provides the physically best access. The stationary slip equation in field-orientated coordinates

$$\omega_r = \frac{I_{sq}}{I_{sd} T_r}$$

can be re-written for the nominal working point and $I_{sd} \approx I_0$ and solved to R_r:

$$R_r \approx \frac{2\pi\left(f_N - \frac{z_p n_N}{60}\right) L_s I_0}{\sqrt{I_N^2 - I_0^2}} \tag{6.74}$$

The stator inductance and the no-load current can be taken from equations (6.71) and (6.72).

6.3.3 Parameter estimation from name plate of PMSM

Starting point for this is the stator voltage equation (cf. [Quang 1996]) in the stationary operation.

$$\begin{aligned} \mathbf{u}_s &= R_s \mathbf{i}_s + j\omega_s L_s \mathbf{i}_s + j\omega_s \boldsymbol{\psi}_p \\ &= R_s \mathbf{i}_s + j\omega_s L_s \mathbf{i}_s + \mathbf{e}_g \end{aligned} \tag{6.75}$$

At the nominal working point and in stationary operation the stator current $\mathbf{i}_s$ only contains the torque-forming component. This fact is represented by the stationary vector diagram in the figure 6.13.

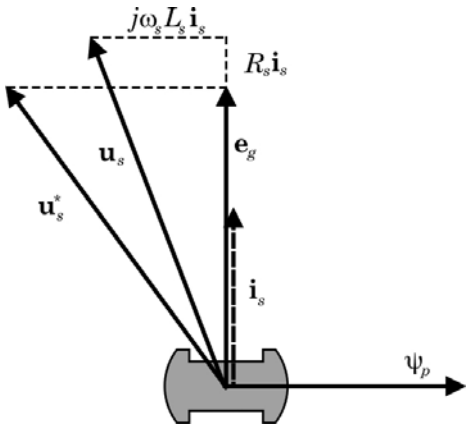

Fig. 6.13 Simplified vector diagram of the PMSM in stationary operation

1. *Calculation of pole flux* $\boldsymbol{\Psi}_p$*:*
   (1) Calculation of torque-forming current: $\hat{I}_{sqN} = \hat{I}_N = \sqrt{2}\, I_N$
   (2) Nominal torque using equation (3.63): $m_N = \frac{3}{2} z_p \psi_p \hat{I}_{sqN}$
   (3) Inserting (1) into (2) it will be obtained: $\psi_p = \frac{2}{3} \frac{m_N}{\sqrt{2}\, z_p I_N}$
2. *Calculation of stator inductance* L_s: The voltage drop over R_s is neglected. The next steps follow from figure 6.13:

(1) Amplitude of nominal voltage: $\hat{U}_N = n_N \sqrt{2}\left(\frac{U_N}{\sqrt{3}}\right)$

(2) Amplitude of EMF: $\hat{\mathbf{e}}_g = 2\pi f_N \psi_p$

(3) After substituting ψ_p the stator inductance L_s is given to:

$$L_s \approx \frac{\sqrt{\hat{U}_N^2 - \hat{\mathbf{e}}_g^2}}{2\pi f_N \hat{I}_{sqN}} \tag{6.76}$$

6.4 Automatic parameter estimation for IM in standstill

6.4.1 Pre-considerations

For the complete description of the IM four parameters are required with a constant parameter model. If the inverse Γ equivalent circuit (cf. fig. 6.3) is chosen as the reference model, the four parameters are then the stator resistance R_s, the rotor resistance R_r, the total leakage inductance σL_s and the stator inductance L_s. The constant parameter model in its precision does not suffice for the synthesis of advanced algorithms, however. At least the inclusion of the saturation characteristics of the inductances is required. Because of the different saturation functions for main and leakage paths a division of the model inductance parameters into leakage inductance σL_s or L_σ and main inductance L_m can be made.

For a current controlled drive the slip is limited also in non-stationary states to values which not yet necessitate a consideration of the current displacement in the rotor for the modelling. Harmonic caused current displacement effects also shall be neglected for the modelling in accordance with the presumptions made (inverter-fed operation at high switching frequency). An exception for the consideration of frequency dependencies is the leakage inductance. Depending on the excitation frequency it has to be distinguished between different inductance values. This means in particular that a transient leakage inductance $\sigma L_s'$ for the current controller design and a stationary (fundamental wave) leakage inductance σL_s for the stator-frequent operation have to be estimated.

The consideration of the iron losses is not avoidable (cf. chapter 7 and 8) for some special tasks. Their identification is practically only possible with the no-load test in a classical way, however, and shall not be discussed more in-depth.

Furthermore, from practical considerations for a useful incorporation of the off-line adaptation into the technological regime of an inverter-fed drive some conditions, which fundamentally narrow down the choice of possible methods, have to be formulated:

1. If possible, no demands or prerequisites on the part of the identification algorithms should be made to technological conditions of the drive. This is the case if the identification runs at standstill and does not need a speed feedback.
2. The safety of the methods and their transferability onto different drive configurations increase if algorithms which run in the closed current control loop are used.

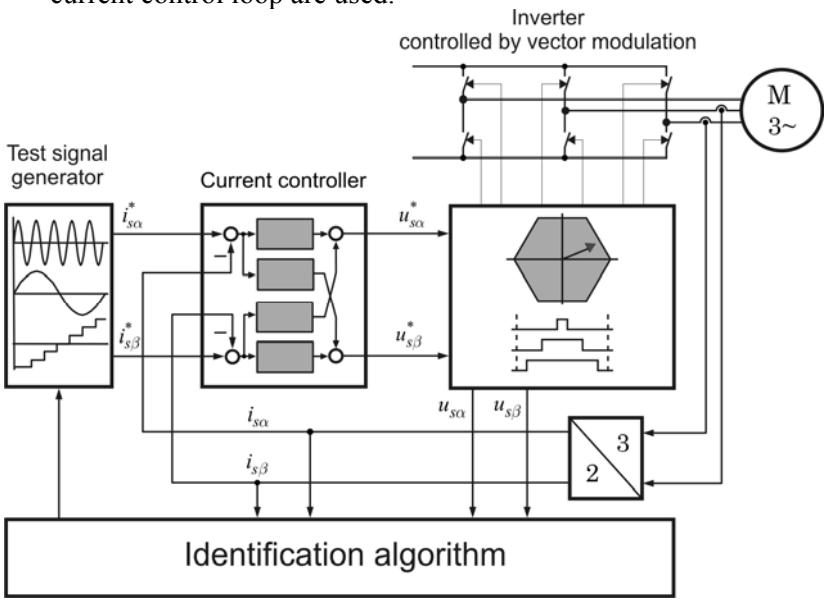

Fig. 6.14 Principle structure of the off-line parameter identification

Regardless that the frequency dependencies are not considered in the model except for the exception mentioned above, the choice of the identification methods has to take into account that such dependencies exist. Thus the test signal frequencies used by the identification should, on one hand, be located in the same range as the frequencies at which the models are operated later. On the other hand the test frequencies have to be selected for current displacement effects not invalidating the identified parameters. For this reason methods with *predefined appropriately selected excitation frequencies* will be preferred for the concrete identification methods in the following sections. The parameter estimation is essentially accomplished by evaluation of the *frequency responses* of

current and voltage. The identification shall be implemented without voltage measuring sensors, and the voltage has to be estimated from the control signals of the inverter.

For the decoupled identification of the parameters, a further criterion for the choice of the excitation frequencies results from the consideration, if possible, not to influence the identification of one parameter by inaccurate other parameters. This suggests to optimize the excitation frequencies by evaluation of sensitivity functions.

The test signals for the parameter identification are produced by frequency inverters. These have a non-linear current-voltage characteristic because of the effects of blanking time, switching delays and voltage drops over the semiconductor switch primarily at small voltages. Just in this voltage area the parameter estimation takes place because of $\omega = 0$. Therefore, the current-voltage characteristic of the inverter must be considered in the model, and also identified for a generally usable identification algorithm. Because of the abandonment of voltage measuring sensors this measure is also imperative for an adequately exact voltage feedback.

The corresponding principle structure of the off-line parameter identification is shown in the figure 6.14.

6.4.2 Current-voltage characteristics of the inverter, stator resistance and transient leakage inductance

As indicated already, a great importance for the precision of the parameter identification for inverter feeding and abandonment of special measuring sensors relies on the voltage capturing. Blanking times and non-linear current-dependent inverter voltage drops have to be considered as error sources which have an effect in particular at small voltages and around current zero crossings. The suppression of their effects on the parameter identification is taken care of in two ways: Firstly by an appropriate choice of the excitation signals, and secondly by embedding the inverter characteristics into the motor model.

Suitable excitation signals are discussed in the context of the individual identification methods specifically. The stator voltage equation is amended by an additional current-dependent term to consider the inverter voltage drops $u_z(i_s)$ in the motor model and looks in the stationary case with $\omega = \omega_s = 0$ as follows:

$$u_s(i_s) = u_z(i_s) + R_s i_s \tag{6.77}$$

At first the measurement of the complete characteristic $u_s(i_s)$ is carried out point wise by impression of DC currents. It has qualitatively the appearance of the dotted curve in figure 6.15. Because of a possible

unbalance of the motor an averaging of the measurements from single tests of the three phases is advisable. Assuming that the voltage increase at high currents is only determined by the linear portions of the voltage drop, the stator resistance can be calculated from the ascent of the current-voltage curve at high current:

$$R_s = \frac{u_{s1} - u_{s2}}{i_{s1} - i_{s2}} \tag{6.78}$$

The then known linear term is now eliminated from (6.77), and the non-linear characteristic remains. For the non-linear inverter voltage drop $u_z(i_s)$ different approaches with constant and/or exponential sections have been proposed in the literature (cf. [Baumann 1997], [Rasmussen 1995], [Ruff 1994]). To avoid the on-line evaluation of exponential functions, a piecewise-linear approximation also can be carried out. A characteristic which also is represented qualitatively in figure 6.15 (solid line) is obtained.

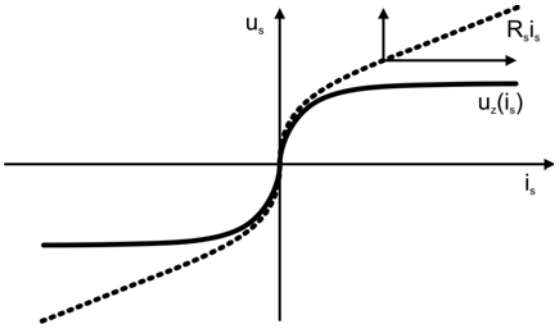

Fig. 6.15 Inverter current-voltage characteristic

The actual compensation is made by a sign and phase correct addition to the voltage reference values, similarly like described in section 2.3.3 for the protection time compensation. With $u_{zu} = u_z(i_{su})$, $u_{zv} = u_z(i_{sv})$ and $u_{zw} = u_z(i_{sw})$ the following voltage components are obtained in stator-fixed coordinates:

$$\begin{aligned} u_{z\alpha} &= \frac{1}{4}\left(2u_{zu} - u_{zv} - u_{zw}\right) \\ u_{z\beta} &= \frac{\sqrt{3}}{4}\left(u_{zv} - u_{zw}\right) \end{aligned} \tag{6.79}$$

To measure the transient leakage inductance a short voltage impulse is applied to the stator winding, and the current gradient is measured. Since the time needed for this test pulse is very short, and the process is barely

noticeable, this measurement can be carried out also outside a special identification run. The leakage inductance arises from:

$$\sigma L_s' = \frac{\hat{u}_s \Delta t}{\Delta i_s} \tag{6.80}$$

For an appropriate width of the voltage pulse and measurement over the complete current slope a good average inductance value will be obtained.

6.4.3 Identification of inductances and rotor resistance with frequency response methods

6.4.3.1 Basics and application for the identification of rotor resistance and leakage inductance

By impressing a sinusoidal current into the stator all desired motor parameters can theoretically be identified by measuring the waveforms of currents and voltages and subsequent frequency response analysis. However, before applying this method some preceding considerations are necessary which follow up the preliminary remarks and determine the most suitable environment.

The demand for an identification at standstill, and therefore the demand that no torque must be developed, can be fulfilled by a single-phase excitation.

The estimation of the stator impedance requires an exact acquisition of the current and voltage fundamental waves. The compensation of the inverter nonlinearities is decisive for the quality of the identification results because of the low voltage amplitudes at standstill (cf. section 6.4.2). Furthermore [Bünte 1995] worked out, that the remaining error only has an effect on the real part of the measured impedance, if the impressed current is sinusoidal. The latter is achieved if the identification is performed in the closed current control loop. Furthermore the current should, if possible, be free of zero crossings because the largest deviations from the sinusoidal form arise in the zero crossings.

A zero crossing free current can be produced by overlaying the sinus reference with a direct current component. This component is reasonably chosen close to the nominal magnetization. This corresponds to a direct current pre-magnetization, and a main field excitation alternating permanently around the working point is produced by the single-phase sinusoidal excitation. Therefore the derivation of the transfer function has to start out from equations of the saturated machine (6.40), (6.41) and (6.43). Because of $\omega = 0$ these equations are simplified to a great deal. In addition, the excitation only takes place in the α axis so that the dimension

of the equation system is reduced to one. Under these prerequisites the following transfer function between stator voltage and stator current can be derived by elimination of i_μ (s = Laplace operator):

$$\frac{u_{s\alpha}}{i_{s\alpha}} = \frac{b_0 + b_1 \mathrm{s} + b_2 \mathrm{s}^2}{1 + a_1 \mathrm{s}} \tag{6.81}$$

$$b_0 = R_s; b_1 = \left(L_m^{'} + L_\sigma\right)\left(1 + \frac{R_s}{R_r}\right)$$

$$b_2 = \frac{L_\sigma}{R_r}\left(L_m^{'} + L_\sigma\right); a_1 = \frac{L_m^{'} + L_\sigma}{R_r}$$

In the steady-state operating condition ($\mathrm{s} \rightarrow j\omega_e$, ω_e ... excitation frequency) the equation (6.81) can be written as a complex impedance:

$$\underline{Z}_s = \frac{\underline{u}_{s\alpha}}{\underline{i}_{s\alpha}} = \frac{b_0 + \left(a_1 b_1 - b_2\right)\omega_e^2}{1 + a_1^2 \omega_e^2} + j\omega_e \frac{b_1 - b_0 a_1 + a_1 b_2 \omega_e^2}{1 + a_1^2 \omega_e^2} \tag{6.82}$$

or

$$\underline{Z}_s = R_s + \frac{R_r\left(\omega_e L_m^{'}\right)^2}{R_r^2 + \omega_e^2\left(L_m^{'} + L_\sigma\right)^2} + j\omega_e\left(L_m^{'} + L_\sigma - \frac{\left(\omega_e L_m^{'}\right)^2\left(L_m^{'} + L_\sigma\right)}{R_r^2 + \omega_e^2\left(L_m^{'} + L_\sigma\right)^2}\right) \tag{6.83}$$

Under special conditions for the excitation frequency the formula (6.83) could further be simplified. For example, with $\sigma\left(\omega_e T_r\right)^2 >> 1$ it can be written:

$$\underline{Z}_s \approx R_s + (1-\sigma)R_r + j\omega_e \sigma L_s \tag{6.84}$$

This equation would be very comfortable for the calculation of the rotor resistance and leakage inductance. The excitation frequency should be within the range of at least 25 Hz, though. Here the current displacement effects in the rotor already have a considerable magnitude and markedly distort the estimated value of the rotor resistance. Under certain assumptions these effects could be taken into account by an additional approach. The safe way, if more than the leakage inductance shall be identified, consists, however, in the evaluation of the complete equation (6.81).

For the estimation of the four parameters of (6.81) current and voltage values have to be captured after achieving the steady-state operating condition over at least one period of the fundamental wave at two excitation frequencies ω_{e1} and ω_{e2}. Harmonics are conveniently

suppressed by discrete Fourier transformation of the measurement values. Two complex resistance values are the result:

$$\begin{aligned}\underline{Z}_{s1}(\omega_{e1}) &= c_1 + jd_1 \\ \underline{Z}_{s2}(\omega_{e2}) &= c_2 + jd_2\end{aligned} \tag{6.85}$$

The coefficients of (6.81) can be calculated as follows:

$$a_1 = \frac{\omega_{e2}d_1 - \omega_{e1}d_2}{\omega_{e1}\omega_{e2}\left(c_2 - c_1\right)} \tag{6.86}$$

$$b_1 = \frac{d_2}{\omega_{e2}} + c_2 a_1 \tag{6.87}$$

$$b_2 = a_1 b_1 + \frac{c_2\left(1 + a_1^2\omega_{e2}^2\right) - c_1\left(1 + a_1^2\omega_{e1}^2\right)}{\omega_{e1}^2 - \omega_{e2}^2} \tag{6.88}$$

$$b_0 = c_1\left(1 + a_1^2\omega_{e1}^2\right) - \omega_{e1}^2\left(a_1 b_1 - b_2\right) \tag{6.89}$$

Solving to the actual machine parameters is elementary. The obtained value for the differential main inductance L_m', however, is not immediately usable because only a small area of the hysteresis curve is passed through at every direct current working point and the gradient at this point does not or only at strong saturation coincide with the gradient of the actual magnetization characteristic. To identify the main inductance the frequency response method has to be adapted specifically (cf. section 6.4.3.3). The value for b_0 contains apart from the stator resistance the uncompensated inverter-caused voltage errors, and is therefore not representative as an estimate.

For the determination of the current dependency of the leakage inductance (saturation characteristic) a separate series of measurements is required because the magnitude of the current must be varied without pre-magnetization. Because of the zero crossing errors the received values differ a little from the leakage inductances found with DC offset. Because no general function for σL_S can be given due to the different leakage saturation behavior, a linear approximation between the test points or a polynomial approximation may be used.

6.4.3.2 Optimization of the excitation frequencies by sensitivity functions

Depending on the excitation frequency, changes of a motor parameter effect the frequency-dependent complex impedance $\underline{Z}_s$ in the equation (6.83) with different strength. This behavior can mathematically be described by the sensitivity function E(*p)* of the complex impedance $\underline{Z}_s$ regarding a parameter *p*. For the separate investigation on the influence on

real and imaginary part of $\underline{Z}_s$, the sensitivity function is calculated one by one for real and imaginary part respectively:

$$\begin{aligned} \mathrm{E_I}(s) &= \frac{\partial \mathrm{Im}(\underline{Z}_s)}{\partial s}\frac{s}{\mathrm{Im}(\underline{Z}_s)} \\ \mathrm{E_R}(s) &= \frac{\partial \mathrm{Re}(\underline{Z}_s)}{\partial s}\frac{s}{\mathrm{Re}(\underline{Z}_s)} \end{aligned} \tag{6.90}$$

After some transformations the following equations result:

$$\mathrm{E_I}(L_m) = \left(1 - \frac{\omega_e^2 L_m'^2 R_r^2\left(3L_m' + 2L_\sigma\right) + \omega_e^4 L_m'\left(L_m' + 2L_\sigma\right)\left(L_m' + L_\sigma\right)^2}{\left(R_r^2 + \omega_e^2\left(L_m' + L_\sigma\right)^2\right)^2}\right)\frac{\omega_e L_m'}{\mathrm{Im}(\underline{Z}_s)} \tag{6.91}$$

$$\mathrm{E_I}(L_\sigma) = \left(1 - \frac{\omega_e^2 L_m'^2\left(R_r^2 - \left(L_m' + L_\sigma\right)^2\right)}{\left(R_r^2 + \omega_e^2\left(L_m' + L_\sigma\right)^2\right)^2}\right)\frac{\omega_e L_\sigma}{\mathrm{Im}(\underline{Z}_s)} \tag{6.92}$$

$$\mathrm{E_I}(R_r) = \frac{2R_r\omega_e^3 L_m'^2\left(L_m' + L_\sigma\right)}{\left(R_r^2 + \omega_e^2\left(L_m' + L_\sigma\right)^2\right)^2}\frac{R_r}{\mathrm{Im}(\underline{Z}_s)} \tag{6.93}$$

$$\mathrm{E_R}(R_r) = \frac{\omega_e^2 L_m'^2\left(\omega_e^2\left(L_m' + L_\sigma\right)^2 - R_r^2\right)}{\left(R_r^2 + \omega_e^2\left(L_m' + L_\sigma\right)^2\right)^2}\frac{R_r}{\mathrm{Re}(\underline{Z}_s)} \tag{6.94}$$

$$\mathrm{E_R}(L_\sigma) = \frac{-2\omega_e^3 L_m'^2\left(L_m' + L_\sigma\right)R_r}{\left(R_r^2 + \omega_e^2\left(L_m' + L_\sigma\right)^2\right)^2}\frac{\omega_e L_\sigma}{\mathrm{Re}(\underline{Z}_s)} \tag{6.95}$$

For reasons which will be discussed in the next section, the sensitivity function of the real part regarding L_m is not of interest. For one example the sensitivity functions are represented in figure 6.16. The typical qualitative characteristic can be transferred and generalized to other motor power ratings.

Values between 2 and 12 Hz prove to be suitable excitation frequencies for the identification of rotor resistance and leakage inductance. The frequencies are still low enough to neglect current displacement effects, on the other side however, adequately high to achieve a decoupling of the main inductance. Optimal values to estimate the main inductance are in the area from 0.1 to 0.4Hz.

An exact pre-computation of optimal excitation frequencies with the help of the sensitivity functions, however, is not possible because these in turn contain the parameters to be identified. But an iterative optimization of the excitation frequencies within several identification runs is possible, thereat no more than 2 - 3 iteration steps are generally required.

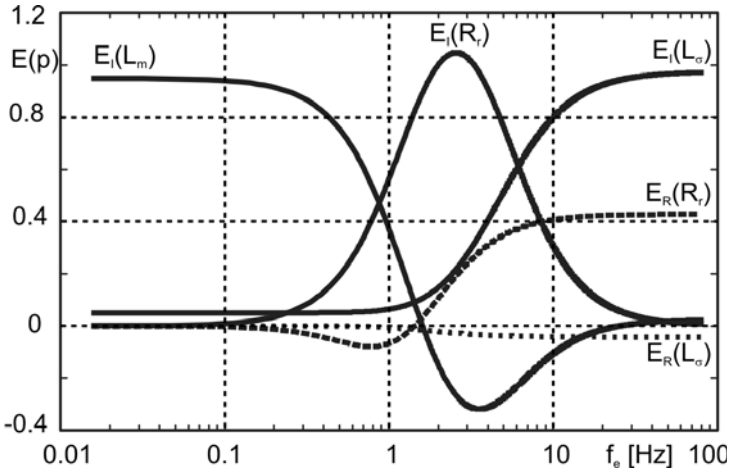

Fig. 6.16 Sensitivity functions of a 3kW motor

6.4.3.3 Peculiarities at estimation of main inductance and magnetization characteristic

Also the main inductance can be identified by single-phase sinusoidal excitation like leakage inductance and rotor resistance. The hysteresis problem mentioned in the previous section can be solved by working without direct current offset. Because of the necessary lower excitation frequencies, zero crossing errors have a less strong effect. Because the voltage measuring errors primarily distort the real part of the measured impedance, only the imaginary part of (6.83) is used for evaluation. Because the imaginary part is mainly determined by the phase shift between current and voltage, this phase shift must be measured with sufficient accuracy which in turn sets a lower limit of approximately 0.1 Hz for the excitation frequency. At this time R_r and L_σ are assumed as known parameters.

Solving the equation (6.83) yields for the main inductance:

$$L_m = \frac{R_r^2 + X_\sigma^2 + 2X_\sigma\left(X_\sigma - \mathrm{Im}(\underline{Z}_s)\right) - \sqrt{\left(R_r^2 - X_\sigma^2\right)^2 - 4\,\mathrm{Im}(\underline{Z}_s)R_r^2\left(\mathrm{Im}(\underline{Z}_s) - 2X_\sigma\right)}}{2\omega_e\left(\mathrm{Im}(\underline{Z}_s) - 2X_\sigma\right)} \tag{6.96}$$

Because the stator current is divided between inductance branch and rotor, the exact magnetization current has to be calculated:

$$i_\mu = i_s \sqrt{\frac{R_r^2 + X_\sigma^2}{R_r^2 + \omega_e^2 \left(L_m + L_\sigma\right)^2}} \tag{6.97}$$

Different operating points on the magnetization characteristic are adjusted by different current amplitudes. It has to be taken into account that the identified main inductance is not identical with the effective main inductance at three-phase excitation. The reason is that the magnetizing current has constant amplitude at three-phase excitation, but changes sinusoidally at single-phase excitation. The amplitudes coincide for the two cases. The voltage at single-phase excitation is distorted due to saturation. *The amplitude of its fundamental wave* evaluated for the frequency response does therefore not represent the instantaneous maximum value of the magnetic field strength correctly. The described relations are qualitatively represented in the figure 6.17.

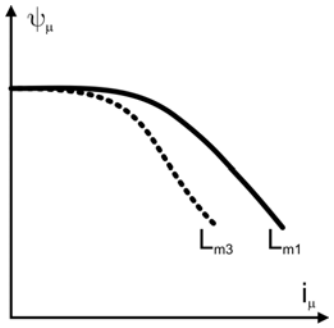

Fig. 6.17 Single-phase and three-phase main inductance

In [Klaes 1992] the difference between single-phase and three-phase inductance is compensated by a constant factor established heuristically which subsequently compresses the scale of the magnetizing current or flux axis. An interesting systematic solution was described in [Bünte 1995]. It assumes that single-phase and three-phase inductance curves $L_{m1}(\hat{I}_\mu)$ and $L_{m3}(i_\mu)$ can be described by polynomials of the n-th degree in the following form:

$$L_{m1}(\hat{I}_\mu) = \sum_{k=0}^{n} a_{1k} \hat{I}_\mu^k \; ; \; L_{m3}(i_\mu) = \sum_{k=0}^{n} a_{3k} i_\mu^k \tag{6.98}$$

The single-phase main inductance L_{m1} is calculated for a sinusoidal magnetizing current $i_\mu(t) = \hat{I}_\mu \sin \omega_e t$ from the continuous Fourier coefficients of the fundamental of the magnetizing current, and the voltage drop over the main inductance u_μ from:

$$\omega_e L_{m1} \int_0^{\pi/\omega_e} i_\mu(t) \sin \omega_e t \, \mathrm{d}t = \int_0^{\pi/\omega_e} u_\mu(t) \cos \omega_e t \, \mathrm{d}t \tag{6.99}$$

Furthermore the following equation applies for the voltage over the main inductance:

$$u_\mu(t) = \frac{\mathrm{d}\psi_\mu}{\mathrm{d}t} = \frac{\mathrm{d}L_{m3}(i_\mu)}{\mathrm{d}t} i_\mu + L_{m3}(i_\mu) \frac{\mathrm{d}i_\mu}{\mathrm{d}t} \tag{6.100}$$

After substituting, processing of integrals and comparison of coefficients the result is:

$$a_{1k} = b_k a_{3k} \quad \text{with} \quad b_k = \begin{cases} 2 \prod_{l=0}^{k/2} \dfrac{2l+1}{2l+2} & \text{for } k \text{ even} \\ \dfrac{4}{\pi} \prod_{l=1}^{(k+1)/2} \dfrac{2l}{2l+1} & \text{else} \end{cases} \tag{6.101}$$

For the above mentioned second method of the adjustment of the characteristic by coordinate axis compression, power-dependent compression factors:

$$i_{\mu 3} = c_k i_{\mu 1} \quad \text{mit} \quad c_k = \sqrt[k]{b_k} \tag{6.102}$$

with values of c_k = 0.85 ... 0.88 for a polynomial degree n = 3 can be derived. Thus this method also should provide a useable characteristic transformation. The polynomial approximation is obtained from the single measurements by applying least squares approximation (cf. section 12.3).

6.4.4 Identification of the stator inductance with direct current excitation

The basic concept of this method is derived from the fact that at impression of a direct current into the stator windings a part of the applied voltage is consumed by the stator resistance, the other part is used to build the stator flux. From the stator voltage equation:

$$u_s = R_s i_s + \frac{\mathrm{d}\psi_s}{\mathrm{d}t} \tag{6.103}$$

and after integration for the stationary state it follows:

$$\int u_s \, \mathrm{d}t = R_s \int i_s \, \mathrm{d}t + L_s i_s \tag{6.104}$$

Because the leakage inductance and the stator resistance are known from the previous measurement, the main inductance can be calculated from that theoretically without difficulty. Offset errors, stationary errors of the voltage measurement or an incorrectly estimated stator resistance can be eliminated, if the integral term on the right side of (6.104) is replaced

by the stator voltage in the steady state condition ($t \to \infty$). In time-discrete notation the computation equation of L_s with the sampling period T, the time step k and the total integration time NT is:

$$L_s = \frac{T\sum_{k=0}^{N} u_s(k) - u_s(\infty)NT}{i_s(\infty)} \tag{6.105}$$

For the determination of the complete magnetization characteristic the identification is realized at different current levels. Because different single tests, particularly at small currents, partly show a considerable scattering of measurements, an averaging of the values from several tests is recommendable. The measurement should be carried out in all three windings to eliminate machine unbalances.

The figure 6.18 shows finally some measurement results. The values for the stator inductance L_s from alternating current and direct current methods delivered by the identification are plotted together with the results of the no-load test. The consequences of voltage measuring errors are most distinctive particularly at small currents and simultaneously small voltage amplitudes. A very good correspondence to the no-load characteristic is shown in the area of high saturation. Altogether, the precision of both methods can be considered as sufficient for the purposes of the self-tuning.

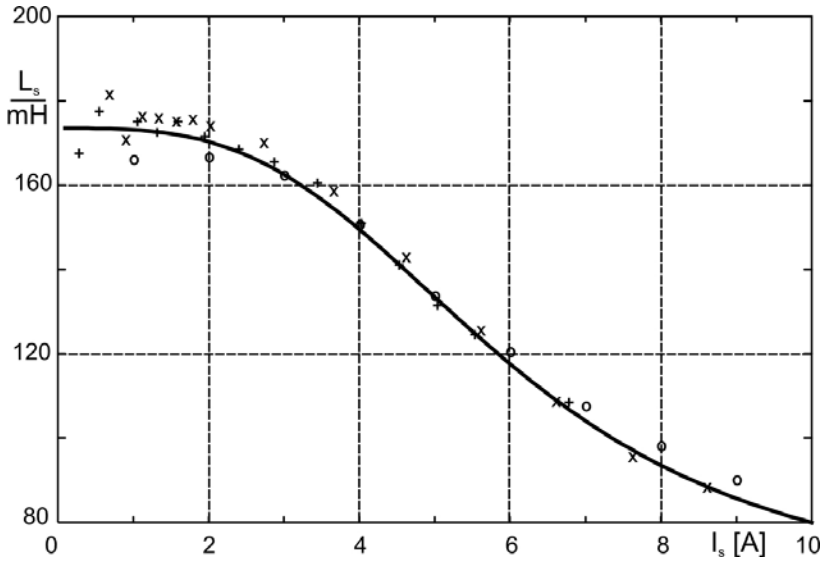

Fig. 6.18 L_s identification for a 5kW motor: no-load test (+), direct current method (o), alternating current method (×), solid line: four-parameter model from no-load measurements (regressed by polynomial of 3rd order)

6.5 References to chapter 6

Baumann T (1997) Selbsteinstellung von Asynchronantrieben. VDI-Fortschritt-Bericht Reihe 21 Nr. 230, VDI Verlag Düsseldorf

Bünte A, Grotstollen H (1995) Offline Parameter Identification of an Inverter-Fed Induction Motor at Standstill. EPE 1995 Sevilla, pp. 3.492 - 3.496

de Jong HCJ (1980) Saturation in Electrical Machines. Proc. of the Intern. Conf. on Electrical Machines, Athen, part 3, pp. 1545 – 1552

Klaes N (1992) Identifikationsverfahren für die betriebspunktabhängigen Parameter einer wechselrichtergespeisten Induktionsmaschine. VDI-Verlag Düsseldorf

Levi E (1994) Magnetic Saturation in Rotor-Flux-Oriented Induction Motor Drives: Operating Regimes, Consequences and Open-Loop Compensation. European Transactions on Electrical Power Engineering Vol. 4, No. 4, July/August, pp. 277 – 286

Lunze K (1978) Einführung in die Elektrotechnik. VEB Verlag Technik Berlin

Murata T, Tsuchiya T, Takeda I (1990) Quick Response and High Efficiency Control of the Induction Motor Based on Optimal Control Theory. 11. IFAC World Congress, Tallin, vol. 8, pp. 242 – 247

Philippow E (1980) Taschenbuch Elektrotechnik, Band 5: Elemente und Baugruppen der Elektroenergietechnik. VEB Verlag Technik Berlin

Quang NP (1996) Digital Controlled Three-Phase Drives. Education Publishing House Hanoi (Book in Vietnamese: Điều khiển tự động truyền động điện xoay chiều ba pha. Nhà Xuất bản Giáo dục Hà Nội)

Rasmussen H, Tonnes M, Knudsen M (1995) Inverter and Motor Model Adaptation at Standstill Using Reference Voltages and Measured Currents. Proceedings EPE 1995 Sevilla, pp. 1.367 - 1.372

Ruff M, Bünte A, Grotstollen H (1994) A New Self-Commissioning Scheme for an Asynchronous Motor Drive System. IEEE Industry Applications Society Annual Meeting Denver, pp. 616 – 623

Schäfer U (1989) Feldorientierte Regelung einer Asynchronmaschine mit Feldschwächung und Berücksichtigung der Eisensättigung und Erwärmung. Dissertation RWTH Aachen

Vas P (1990) Vector Control of AC Machines. Oxford University Press

Vogt K (1986) Elektrische Maschinen, Berechnung rotierender elektrischer Maschinen. VEB Verlag Technik Berlin